Parameter Identification for Nonlinear Circuit Models of Power BAW Resonators

Florin CONSTANTINESCU[1], Alexandru Gabriel GHEORGHE[1], Miruna NITESCU[1], Aurelian FLOREA[1], Olivier LLOPIS[2], Petrica TARAS[1]
[1]*Department of Electrical Engineering, Politehnica University, Spl. Independentei nr. 313, Bucharest, Romania*
[2]*Laboratoire d'Analyse et d'Architecture des Systemes, 7, av. du colonel Roche, 31077 Toulouse, France*
florin.constantinescu@lce.pub.ro

***Abstract*—The large signal operation of the bulk acoustic wave (BAW) resonators is characterized by the amplitude-frequency effect and the intermodulation effect. The measurement of these effects, together with that of the small signal frequency characteristic, are used in this paper for the parameter identification of the nonlinear circuit models developed previously by authors. As the resonator has been connected to the measurement bench by wire bonding, the parasitic elements of this connection have been taken into account, being estimated solving some electrical and magnetic field problems.**

Index Terms—**BAW resonators and filters, radiofrequency microelectromechanical systems, radio transceivers, radiofrequency integrated circuits, circuits for communications.**

I. INTRODUCTION

In the last years, the BAW AlN resonators emerged as a very efficient solution for mobile communications filters due to the possibility to be integrated at a relatively low cost together with CMOS circuits in systems on a chip and systems in a package.

As these resonators are used for designing mobile communication filters, which in turn are incorporated in RF circuit blocks, a circuit model of this kind of device is very useful. For small signal operation, the BVD circuit (Fig. 1.a) is a very good model in a narrow frequency band containing the series and parallel resonance frequencies f_s and f_p (Fig. 1.b).

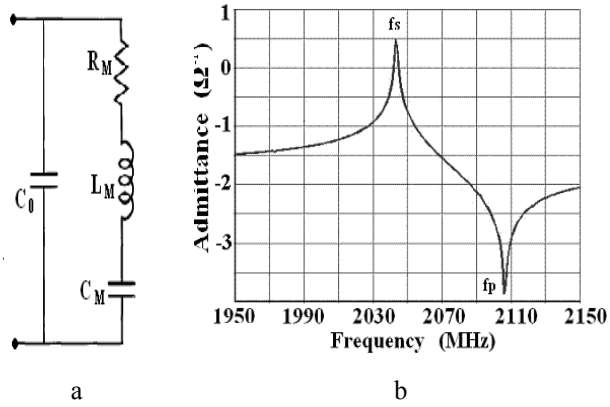

Figure 1. Small signal operation a) Butterworth Van Dyke (BVD) circuit, b) admittance vs. frequency

The power BAW AlN resonators have a large signal operation characterized by two nonlinear effects [1]: the amplitude-frequency effect and the intermodulation effect. The amplitude-frequency effect of an AlN resonator means that the values of f_s and f_p decrease as the input power increases, while the presence of the 2f and 3f components in the response to a sinusoidal excitation with frequency f illustrates the intermodulation effect.

Some circuit models which reproduce the amplitude-frequency effect are proposed in [2, 3]. They modify the linear BVD circuit in Fig 1.a, R_M and C_M having polynomial dependences on the r.m.s. value of the first harmonic in the resonator current. A parameter identification procedure for these models is given in [4].

These linear parametric models can reproduce the amplitude-frequency effect but don't give intermodulation products. As the frequency domain simulators like APLAC and ADS do not allow r.m.s. values as model variables, these models cannot be implemented in this kind of simulators. Because a r.m.s. value may be computed only after an excitation period is swept, the linear parametric models cannot be implemented in time domain simulators as SPICE and SPECTRE, too.

The circuit models for power BAW resonators having elements with polynomial nonlinearities suggested in [5] have been developed in [6, 7]. The first nonlinear model has the same structure as the BVD circuit.

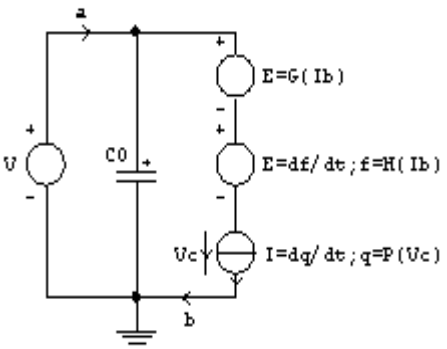

Figure 2. Controlled source implementation of the first nonlinear circuit model

Its APLAC implementation using nonlinear controlled sources is given in Fig. 2. Considering the following

This work has been supported by the IDEAS project No. 2198 financed by the National Council of Scientific Research in Higher Education (Romania) and by the European project MOBILIS.

Digital Object Identifier 10.4316/AECE.2011.01009

parameter values
C0 = 1.566e-12
CCVS R1 1 2 1 b [4.7*(CI(0)+0.5*CI(0)^2 +0.5*CI(0)^3)] R
CCVS L1 2 3 1 b [3.5e-9*(CI(0)-5e-2*CI(0)^2+1e-2*CI(0)^3)] L
VCCS C1 3 5 1 3 5 [.177e-12*(CV(0)+1e-2*CV(0)^2+1e-4*CV(0)^3)] C
the amplitude-frequency effect in the vicinity of f_s is illustrated in Fig. 3.

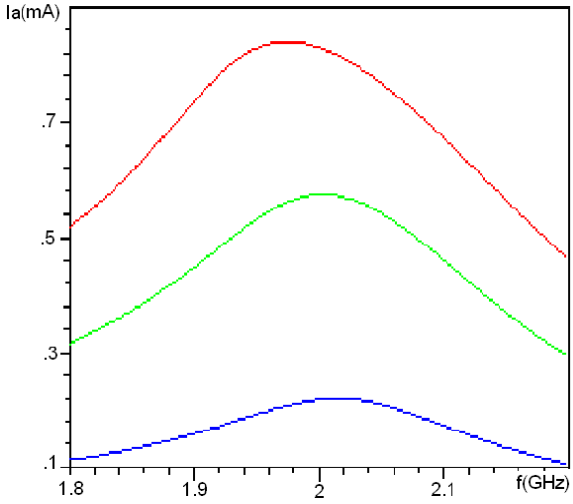

Figure 3. Ia vs. frequency for the first nonlinear model

The three curves shown in this figure correspond to V=1V (blue), V=3V (green), and V=5V (red). The intermodulation effect, namely the second and third harmonic components for three frequencies, is shown in Fig. 4.

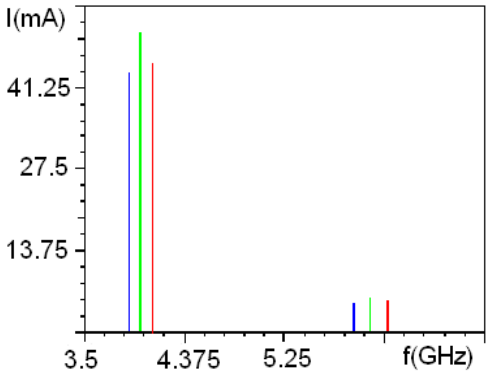

Figure 4. Intermodulation products for V=5V, first model

Forcing the current value in the motional branch by means of the VCCS, the capacitor has a dominant role in this model, both the resonance frequency shift and the amplitudes of the intermodulation products depending mainly on its nonlinear characteristic. To avoid this disadvantage a second model is proposed (Fig. 5).

A similar nonlinear control source implementation is made in APLAC. Using the parameters:
Res Ri 4 6 1
CCVS L1 1 2 1 b [3.5e-9*(CI(0)+1e-1*CI(0)^2+1e-2*CI(0)^3)] L
CCVS R1 3 5 1 c [430*(CI(0)+2e-2*CI(0)^2+2e-2*CI(0)^3)] R
VCCS C1 3 GND 1 3 GND [.177e-12*(CV(0)+5e-5*CV(0)^2+5e-5*CV(0)^3)] C
an amplitude-frequency effect similar to that in Fig. 3 is obtained. The intermodulation effect is illustrated in Fig. 6, while, modifying the inductor parameters as

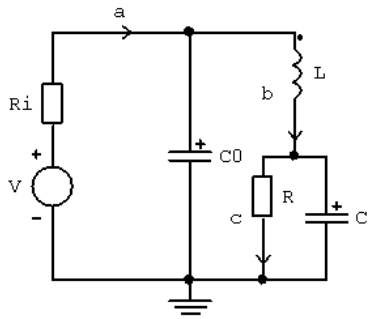

Figure 5. Second circuit model

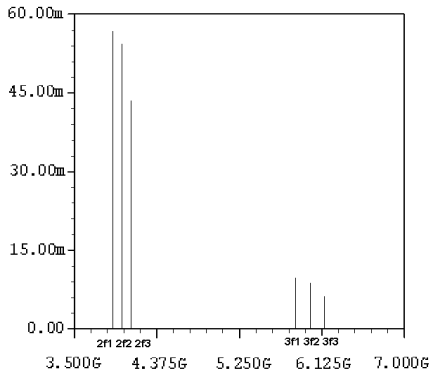

Figure 6. Intermodulation products for V=5V, second model

CCVS ...[3.5e-9*(CI(0)+1e-3*CI(0)^2+1e-3*CI(0)^3)] L
the second harmonic is practically vanished (fig. 7), the amplitude-frequency effect remaining unchanged.

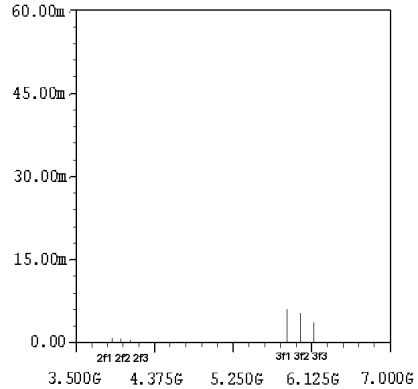

Figure 7. Intermodulation products for V=5V, second model, modified inductor parameters

In [7], due to the lack of experimental results for the intermodulation effect, the first model parameters have been fitted in order to comply with the amplitude-frequency effect measurements only.

For the first time in the literature, the parameter identification for these nonlinear circuit models, taking into account both amplitude-frequency and the intermodulation effects, is presented in this paper. Section II presents the procedure used for the measurement of these two effects. The influence of the parasitic elements of the resonator

connection to the measurement bench is considered in Section III, the parameter identification being performed in Section IV.

II. Measurement Method

A picture of the measurement bench is given in Fig. 8. Bottom left we have a vector network analyzer (VNA) used to measure the S-parameters of the BAW resonator at various power levels. On top we have a spectrum analyzer, which measures the second and third harmonic components. The input sinusoidal signal is generated by the VNA source, which is connected at the port 1 of the measurement circuit. This source gives sets of 800 signals of the same power and various frequencies in the band of interest in order to measure the amplitude-frequency effect. The source signal is amplified by a 30W amplifier which has a linear operation, the maximum output used in the measurements being 6.4W. Moreover, a low pass filter has been added, just to be sure that no second or third harmonic generated by the amplifier will be added to the incident wave reaching the resonator. Before reaching the resonator, the amplified signal passes through a bidirectional coupler. The BAW resonator is a one-port connected to the coupler. The coupler returns the reflected wave to the input of VNA (port 2 of the measurement circuit). VNA measures the real and imaginary parts of S_{21} in the measurement circuit. The $S^{D}_{11\_}$ parameter of the device under test (DUT- the BAW resonator) is computed using a "thru" calibration software. To this end two measurements are performed whose results are $S_{21\ open}$ (DUT is replaced by an "open") and S_{21_DUT} (DUT is connected in the measurement circuit). Both DUT and "open" are contained in similar connection devices which are aimed to connect them with a coaxial cable. The "open" has no connection wires, unlike DUT.

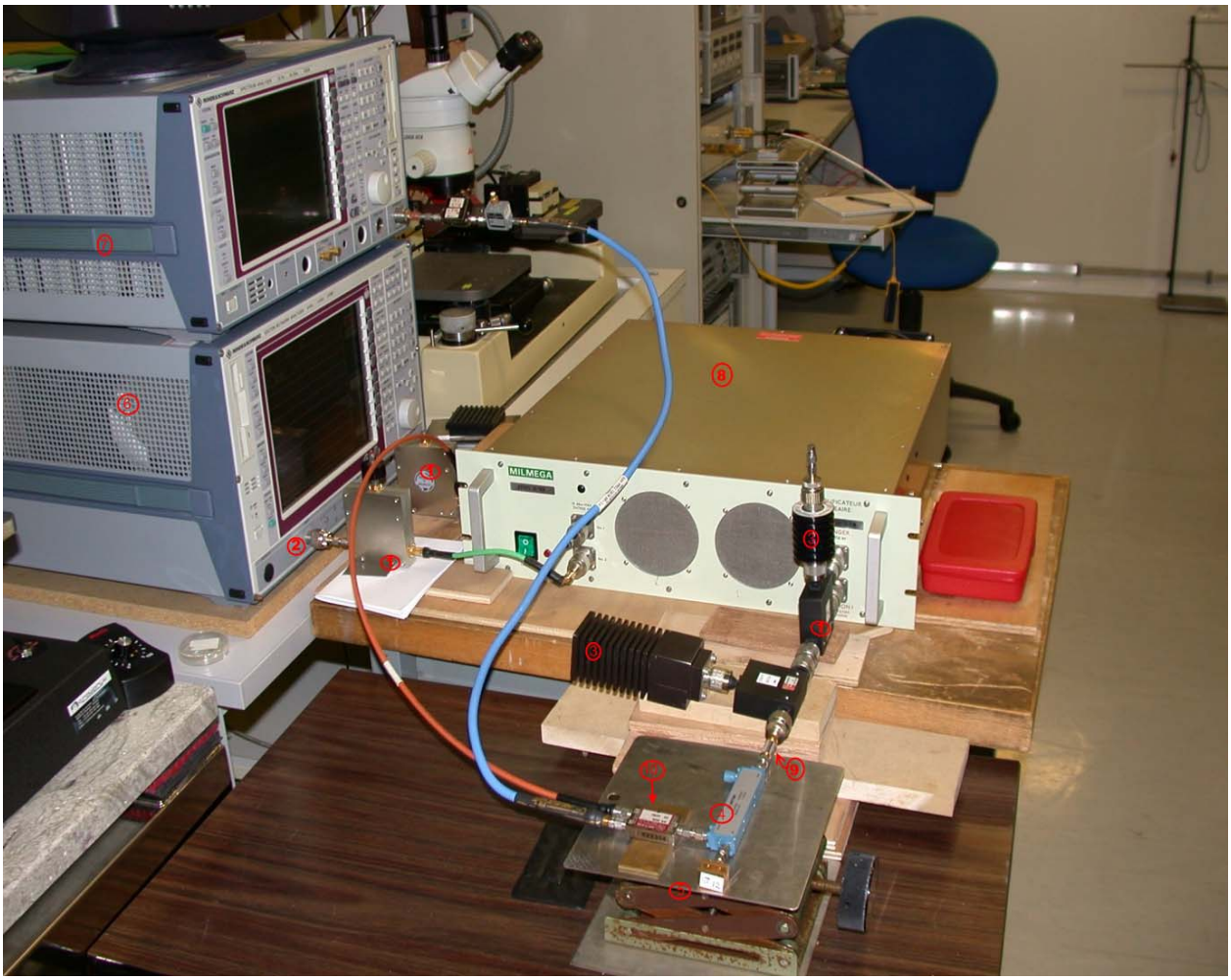

Figure 8. Measurement bench

As the level of the third harmonic component is close to or under the noise floor [8], only the second harmonic will be considered for the parameter identification in Section IV.

Six resonators, built with the same layers, have been measured; three of them having square upper electrodes, the other three being apodized in order to avoid influence of the lateral modes. Nevertheless, a strange frequency dependence of the second harmonic component has been observed (Fig. 16) even if the resonator is apodized. A similar result has been reported in [9].

The measurements results will be presented in Section 4, together with the model simulation results.

III. Equivalent Circuit of the Connection to the Measurement Bench

The DUT can be connected to the measurement bench by two ways: a GSG (ground-signal-ground) probe or wire bonding (a wire connection for each one of the GSG

contacts). The former solution allows the elimination of the connection parasitics influence via calibration, but destroys DUT contacts in the case of multiple measurements. The later one allows multiple measurements in exactly the same conditions but its parasitics due to the connection wires cannot be compensated by calibration. Our measurements have been performed using wire bonding.

The connection wires of our DUT are given in Fig. 9. The longest dimension of the connection wire system is smaller than 2mm. As the wavelength corresponding to our central frequency of operation (2GHz) is $\lambda=c/f=3\ 10^8/2\ 109= 150$ mm >> 2mm, a lumped circuit model of the connection wires can be built.

The central wire (red) connects the S pad to the central wire of the connection structure. The G pads are connected to the ground (the blue plane in Fig. 9) via two wires (blue).

This wire system exhibits inductive, capacitive and resistive effects. The most important one is the inductive effect which can be computed assuming the current I flowing through the red wire and I/2 currents flowing through the blue wires. Computing the magnetic energy W_m it follows that the parasitic inductance is $L_p= 2\ W_m/I^2$. The parasitic capacitance is computed using the model in Fig. 9 as $C_p=2\ W_e/V^2$, where V is the voltage between the red wire and ground and W_e is the electrical energy of the wire system. The parasitic resistance R_p is computed taking into account the wires dimensions and the skin depth.

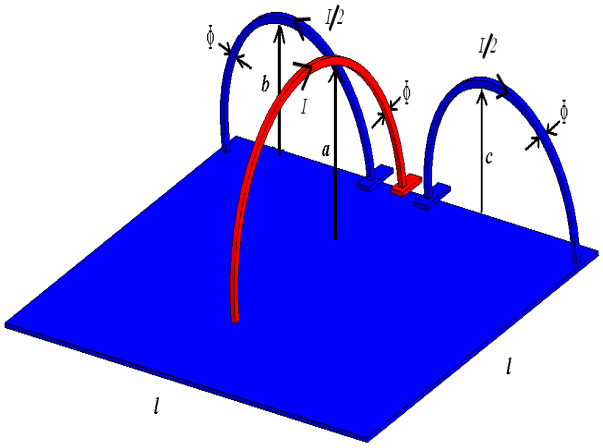

Figure 9. Connection wires model

The equivalent circuit of the wire system is given in Fig. 10. Terminal 1 is connected to the central wire of the connection device while terminal 2 is connected to the S pad of the resonator.

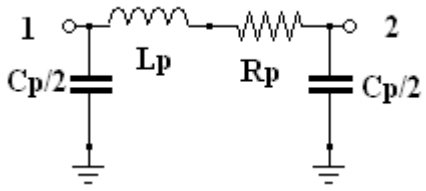

Figure 10. Equivalent circuit of the connection to the measurement bench

IV. Circuit Models

The parameters of the nonlinear circuit models for two SMR power BAW resonators are identified in this section. The die containing the test resonators has the same continuous layers except the upper electrodes. Taking into account that the thickness mode of propagation of the acoustic waves is dominant, it follows that f_s and f_p values don't depend in principle on the resonator area. Nevertheless, the lateral modes and layer thickness non-uniformity can influence these values as well as other resonator characteristics.

The parameters of the BVD circuit, modeling the small signal operation can be determined, starting from the known values for f_s, f_p, and Q_s (quality factor at f_s), using a procedure including the following steps [10]:

-computation of the low frequency capacity $C_{LF}=C_0+C_M$ by solving an electrostatic field problem,

-computation of the coupling coefficient $k^2 = \dfrac{f_p^2 - f_s^2}{f_p^2}$,

-computation of $C_0 = C_{LF}(1-k^2)$ and $C_M = C_{LF}k^2$,

-computation of $L_M = 1/(\omega_s^2 C_M)$

-computation of $R_M = 1/(Q_s C_m \omega_s)$

The low frequency capacity is computed for a square resonator whose upper electrode edge is ***a*** (Fig. 11, the lower part). The upper part of the drawing is a detail of the corner of the lower part. This model takes into account only the upper electrode (orange) and the piezoelectric layer (green). The boundary conditions are V=1 on the electrode surface and V=0 on the lower face of the dielectric. A quarter of the resonator is taken into account using symmetry boundary conditions. The dielectric is AlN having ε=82.6 pF/m and the edge length 3a.

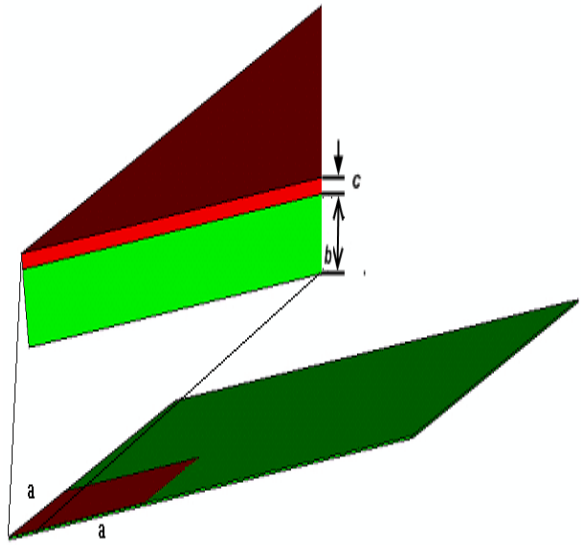

Figure 11. Model for the computation of C_L

The capacity corresponding to a=150μm, c=0.24μm and b= 1.17μm has been computed, the other capacity values being estimated taking into account the proportionality with the electrode area.

The measured values f_s and f_p are the resonance frequencies of the assembly formed by the connection

device, connection wires, and the resonator itself. These values are influenced more or less by the parasitics of the connection wires. As the connection wires are mounted manually, their influence cannot be compensated by calibration, unlike the influence of the connection device.

The parameters of two resonators are identified in the following. The first resonator, having a relatively small area determining a relatively high impedance value, has the measured values f_s and f_p slightly influenced by the parasitics of the connection wires, while the second one having a relatively large area (which determines a relatively low impedance value) exhibits a strong influence of these parasitics on the measured values f_s and f_p.

Resonator A

This is an apodized resonator having an area of 22100 μm^2 with the connection wires model in Fig. 9 defined by a=400µm, b=300µm, c=300µm, Φ=20µm, l=1500µm. It follows that C_{LF}=1.824pF. The skin depth in the gold wires at the central frequency of 2GHz being 1.9106 µm, the parameters of the parasitic elements are given in Fig. 12. C_{LF}, L and C have been obtained using the electromagnetic field solver FLUX 3D. C_{LF} and C have been computed by solving electrostatic field problems, while L has been calculated by solving a stationary magnetic field problem.

The first nonlinear circuit model has been used in this case, its parameters being given in Fig. 12. These parameters have been computed assuming f_s=2.0331GHz, f_p=2.0815GHz and Q_s=227.73.

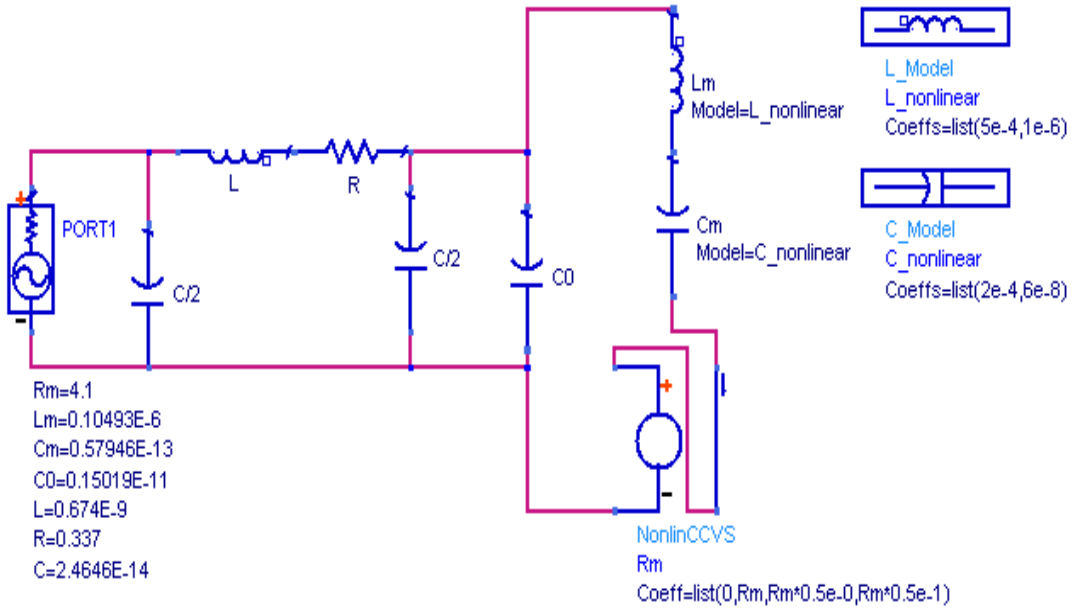

Figure 12. Nonlinear circuit model of the resonator A

All circuit simulations reported in this Section are made with ADS.

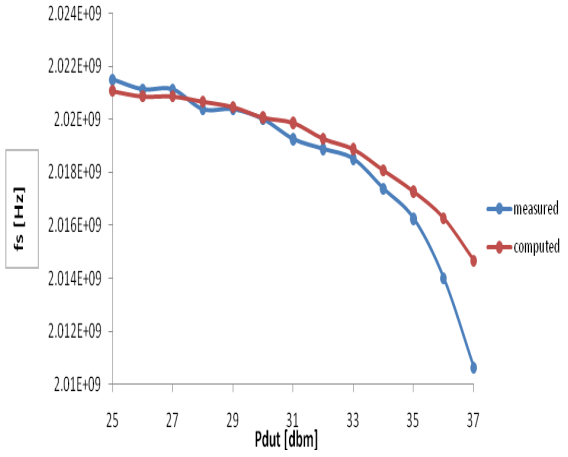

Figure 13. Measured and computed dependence of f_s on P_{dut} for the resonator A

The coefficients of the polynomial nonlinear characteristics for L_m, C_m, and R_m have been fitted in order to comply with the measured values of f_s and f_p as functions of the incident power P_{dut}.at resonator terminals (Fig. 13, Fig. 14).

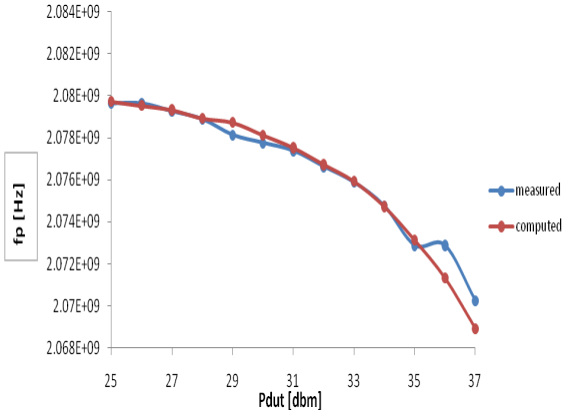

Figure 14. Measured and computed dependence of f_p on P_{dut} for the resonator A

A very good agreement between the measured and

simulated data has been observed in both Fig. 13 and Fig. 14. The measured and simulated frequency characteristics of the admittance modulus for this resonator are given in Fig. 15 for two values of P_{dut}. The very good agreement between the measured and simulated characteristics is obvious.

The intermodulation effect is taken into account for the second harmonic only. The measured and computed values for the 2f reflected power are given in Fig. 16.

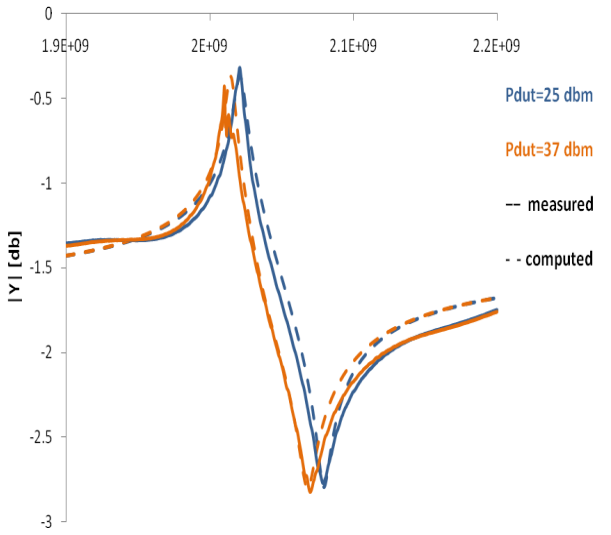

Figure 15. Measured and computed frequency characteristics of the resonator A

The measured values have some local minima and maxima unlike the simulated values. These undulations can be explained taking into account the influence of lateral modes of propagation, which exist, even for the apodized resonators. A similar effect has been reported in [9].

Except this aspect, the agreement between measured and simulated data can be considered as good.

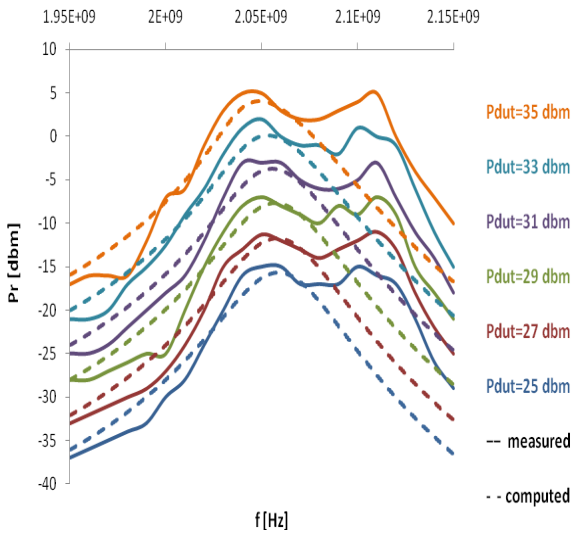

Figure 16. Measured and computed frequency dependence of the 2f reflected power for the resonator A

Resonator B

This is an apodized resonator having an area of 90000 μm^2 with the connection wires model in Fig. 9 defined by a=350µm, b=300µm, c=235µm, Φ=20µm, l=1500µm.

It follows that C_{LF}=7.296pF. The values of the parasitic elements are given in Fig. 17.

The second nonlinear circuit model has been used in this case, its parameters being given in Fig. 17. These parameters have been computed assuming f_s=2.04GHz, f_p=2.0855GHz and Q_s=330.35.

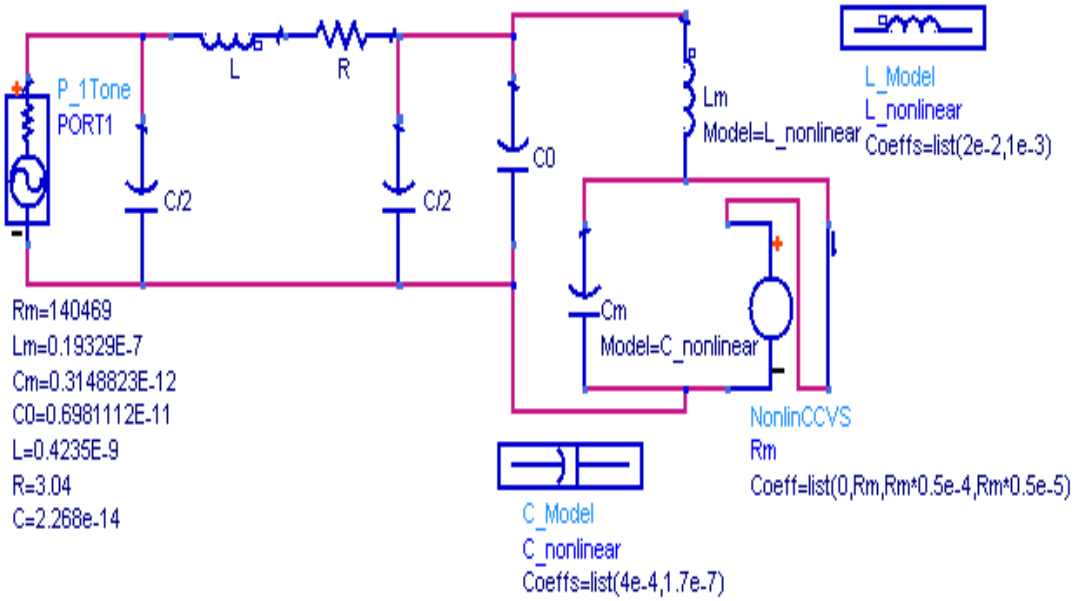

Figure 17. Nonlinear circuit model of the resonator B

The coefficients of the polynomial nonlinear characteristics for L_m, C_m, and R_m have been obtained in a similar manner to the first example.

Unlike the previous case, the simulated dependence of f_s on P_{dut} is not close to the measured data (Fig. 18). A possible reason is a calibration error corresponding to the use for this resonator of a connection device which is slightly different to that of the "open". If these two

connection devices were identical, their effect would be compensated by calibration, as it happens for the resonator A. The measured and computed dependence of f_p on P_{dut} are in a very good agreement (Fig. 19). Perhaps the calibration error refers to a series impedance whose module is negligible with respect to the very high impedance module of the resonator itself near f_p.

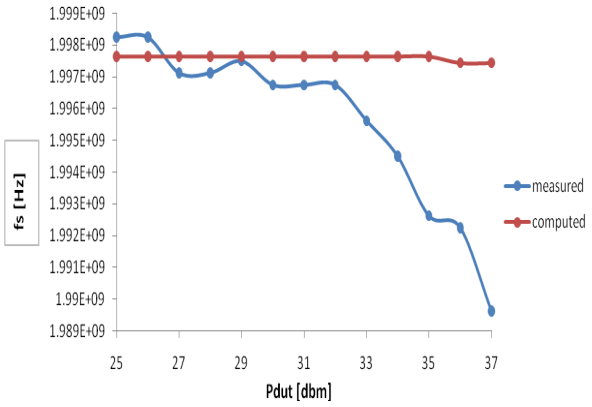

Figure 18. Measured and computed dependence of f_s on P_{dut} for the resonator B

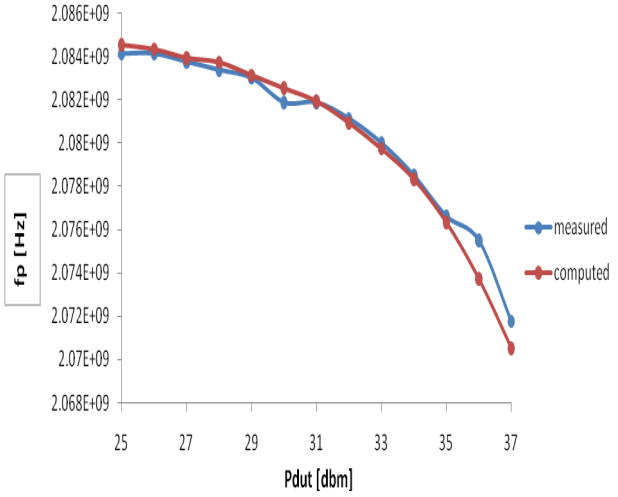

Figure 19. Measured and computed dependence of f_p on P_{dut} for the resonator B

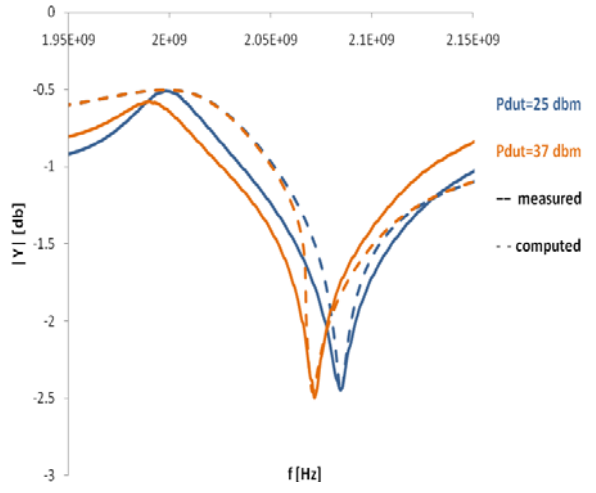

Figure 20. Measured and computed frequency characteristics of the resonator B

The above mentioned aspects can be observed in the frequency characteristics shown in Fig. 20, also.

The measured and computed values for the 2f reflected power are given in Fig. 21. An acceptable agreement between the measured and simulated data can be observed.

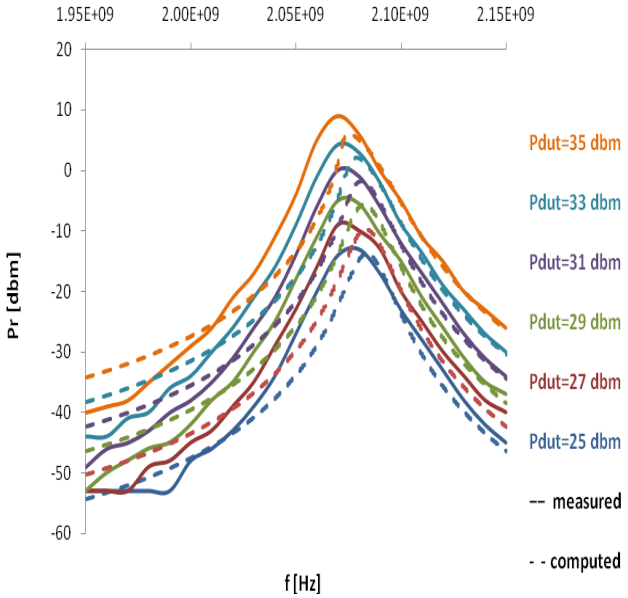

Figure 21. Measured and computed frequency dependence of the 2f reflected power for the resonator B

The local maxima and minima given in Fig. 16 are not visible, the influence of the lateral modes being negligible due to the greater area of this resonator.

V. Conclusion

The parameters of the nonlinear circuit models of power BAW resonators developed in [6] have been identified in this paper using the measurements of the amplitude-frequency effect and of the intermodulation effect. Only the 2f harmonic components have been used because the level of the 3f harmonic components is close to or under the noise floor. To the authors knowledge, this is the first time when the parameters of a nonlinear circuit model of a BAW resonator are identified taking into account the measurements of the two nonlinear effects mentioned above.

The measurements being performed using wire bonding, the influence of the connection wires which are mounted manually cannot be compensated by calibration. This is why a lumped circuit model of these wires has been developed using the electromagnetic field solver FLUX 3D.

The model of the first resonator gives results which are in a very good agreement with the measurements except some undulations in the frequency characteristic of the second harmonic of the reflected power. These undulations can be explained by the influence of the lateral modes which are significant in a small area apodized resonator, a similar experimental result being obtained in [9].

The model of the second resonator shows a good agreement with the measured dependence of f_p on the incident power and an acceptable agreement with the measured frequency characteristic of the second harmonic of the reflected power; this last characteristic exhibits no undulations, the lateral modes being attenuated due to a four times larger surface than that of the first resonator. The

simulated dependence of f_s on the incident power is not close to the measured data, perhaps due to a calibration error which is negligible around f_p, due to the high value of the resonator impedance in the vicinity of this frequency.

These nonlinear circuits are reduced complexity behavioral models which, due to their small number of circuit elements, can be used very efficiently in simulation of microelectronic circuits including BAW resonators. These models can be employed in the design of power BAW filters used in circuits and systems for communications [1, 10]. Their parameters having not an explicit dependence on the characteristics of the layers contained by the BAW resonators, these models are not suitable for the physical design. To this end physical models must be used, like the nonlinear artificial transmission line containing hundreds of circuit elements [11]. Both behavioral and physical models can be used in building design kits for MEMS which will allow faster design cycles better optimized for the specific technology that is used [12].

ACKNOWLEDGMENT

The authors would like to thank prof. V. Fireteanu, prof. I. F. Hantila, and prof. M. Maricaru for the helpful discussions.

REFERENCES

[1] R. S. Ketcham, G. R. Kline, K. M. Lakin, "Performance of TFR filters under elevated power conditions", *42-nd Annual Frequency Control Symposium* (1988), pp. 106-111.

[2] J. Nosek, "Drive level dependence of the resonant frequency in BAW quartz resonator and his modeling", *IEEE Trans. on Ultrasonics, Ferroel. and Freq. Control*, 46, pp. 823- 829, July 1999..

[3] Albareda, P. Gonnard, V. Perrin, R. Briot, D. Guyomar, Characterization of the mechanical nonlinear behavior of piezolelectric ceramics. *IEEE Trans. on Ultrasonics, Ferroel. and Freq. Control*, 47: 844- 853.

[4] M. Nitescu, F, Constantinescu, A. G. Gheorghe "An AC parametric behavioral model of a nonlinear BAW resonator", *Proc. 2008 European Conference on Circuits and Systems for Communications*, Bucharest, Romania, pp 176-179.

[5] R. Aigner, N.- H. Huynh, M. Handtmannn, S. Markensteiner, Behavior of BAW devices at high power level, *Proc. 2004 IEEE MTT-S International Microwave Symposium.*

[6] F. Constantinescu. M. Nitescu, A. G. Gheorghe, "Circuit models for power BAW resonators –set-up and implementation", in *Proc. AFRICON 2007*, Windhoek, Namibia, September 26-28 2007.

[7] F. Constantinescu. M. Nitescu, A. G. Gheorghe, "New circuit models for power BAW resonators ", in *Proc. ICCSC 2008,* Shanghai, China, pp.176-179.

[8] S. Godet, S. Gribaldo, E. Tournier, O. Llopis, A. Reinhardt, J.B. David, "An automated measurement bench for integrated BAW resonators nonlinear characterization at microwave frequencies", *Proc. European Frequency and Time Forum*, EFTF 2008, Toulouse, April 2008.

[9] N. Ben Hassine, D. Mercier, P. Renaux, "Solidly mounted resonators under high power - study for reliability assessment", *5th* International *Conference on Ph.D. Research in Microelectronics & Electronics*, 12-17 July 2009 - Cork, Ireland.

[10] M. R. Islam, J. Kim, "Cooperative techniques based on sensor selection in wireless sensor network", *Advances in Electrical and Computer Engineering*, vol. 8 (2009), No. 1, pp. 56-62.

[11] [11] F. Constantinescu. A. G. Gheorghe, A. Florea, M. Nitescu, O.Llopis, Artificial transmission line model for power BAW resonators, Revue Roum. Sci. Techn., Ser. Electrotechn et Energ., 2011 (to appear).

[12] [12] J. Hogan, The democratization of MEMS design and manufacturing, Microwave Engineering Europe, September 2010, www.microwave-eetimes.com, pp. 34-35.